Title: A trans-envelope complex maintains outer membrane lipid homeostasis via retrograde phospholipid transport in *Escherichia coli*

Authors: Rahul Shrivastava[a], Xiang'Er Jiang[b], Shu-Sin Chng[a,b*]

Affiliations:

[a]Department of Chemistry, National University of Singapore, Singapore 117543.

[b]Singapore Center for Environmental Life Sciences Engineering, National University of Singapore (SCELSE-NUS), Singapore 117456.

*To whom correspondence should be addressed. E-mail: chmchngs@nus.edu.sg

Author contributions: R.S. performed all experiments described in this work; X.E.J. performed experiments related to LpxC overexpression; R.S. and S.-S.C. analyzed and discussed data; R.S. and S.-S.C. wrote the paper.

The authors declare no conflict of interest.

Running title: Outer membrane homeostasis via retrograde lipid transport

Classification

Biological Sciences – Microbiology and Biochemistry

Abstract

The outer membrane (OM) is essential for viability in Gram-negative bacteria. It also serves as a formidable permeability barrier against external insults, such as antibiotics and bile salts, thus allowing cells to survive in harsh environments. Biogenesis of the OM requires the coordinated transport and assembly of proteins and lipids, including lipopolysaccharides (LPS) and phospholipids (PLs), into the membrane. While pathways for LPS and OM protein assembly are well-studied, how PLs are transported to and from the OM is not clear. Mechanisms that ensure OM stability and homeostasis are also unknown. The trans-envelope Tol-Pal complex, whose physiological role has remained elusive, is important for OM stability, and for proper OM invagination during cell division. Here, we establish the function of the Tol-Pal complex in PL transport and OM lipid homeostasis in *Escherichia coli*. Cells lacking the complex exhibit defects in lipid asymmetry and accumulate excess phospholipids (PLs) in the OM. This imbalance in OM lipids is due to defective retrograde PL transport in the absence of a functional Tol-Pal complex. Thus, cells ensure the assembly of a stable OM by maintaining an excess flux of PLs to the OM only to return the surplus to the inner membrane via transport mediated by the Tol-Pal complex. Our findings also provide insights into the mechanism by which the Tol-Pal complex promotes OM invagination during cell division.

Keywords

outer membrane stability; membrane homeostasis; lipid trafficking; membrane lipid asymmetry; membrane contact sites; TolQRA

Significance statement

Biological membranes define cellular boundaries, allow compartmentalization, and represent a prerequisite for life; yet, our understanding of membrane biogenesis and stability remain rudimentary. In Gram-negative bacteria, the outer membrane prevents entry of toxic substances, conferring intrinsic resistance against many antibiotics. How the outer membrane is assembled, and stably maintained, are not well understood. In this study, we established the role of a trans-envelope protein complex in outer membrane lipid homeostasis, and demonstrated that this complex is functionally important for phospholipid transport. Our work provides fundamental understanding of lipid trafficking within the Gram-negative double-membrane envelope in the context of membrane assembly and homeostasis. Furthermore, it highlights the importance of exploiting lipid transport processes as targets for the development of future antibiotics.

Introduction

Lipid bilayers define cellular compartments, and thus life itself, yet our understanding of the assembly and maintenance of these structures are limited. In Gram-negative bacteria, the outer membrane (OM) is essential for growth, and allows the formation of an oxidizing periplasmic compartment beyond the cytoplasmic or inner membrane (IM) (1). The OM is asymmetric, with lipopolysaccharides (LPS) and phospholipids (PLs) found in the outer and inner leaflets, respectively. This unique lipid asymmetry is required for the OM to function as an effective and selective permeability barrier against toxic substances, rendering Gram-negative bacteria intrinsically resistant to many antibiotics, and allowing survival under adverse conditions. The assembly pathways of various OM components, including LPS (2), β-barrel OM proteins (OMPs) (3), and lipoproteins (4), have been well-characterized; however, processes by which PLs are assembled into the OM have not been discovered. Even though they are the most basic building blocks of any lipid bilayer, essentially nothing is known about how PLs are transported between the IM and the OM. Unlike other OM components, PL movement between the two membranes is bidirectional (5-7). While anterograde (IM-to-OM) transport is essential for OM biogenesis, the role for retrograde (OM-to-IM) PL transport is unclear. How assembly of the various OM components are coordinated to ensure homeostasis and stability of the OM is also unknown.

The Tol-Pal complex is a trans-envelope system highly conserved in Gram-negative bacteria (8, 9). It comprises five proteins organized in two sub-complexes, TolQRA in the IM and TolB-Pal at the OM. In *Escherichia coli*, these sub-complexes interact in a proton motive force (pmf)-dependent fashion, with TolQR transducing energy to control conformational changes in TolA and allowing it to reach across the periplasm to contact Pal (10, 11), an OM

lipoprotein that binds peptidoglycan (12). TolA also interacts with periplasmic TolB (13), whose function within the complex is not clear. The TolQRA sub-complex is analogous to the ExbBD-TonB system (8, 14, 15), where energy-dependent conformational changes in TonB are exploited for the transport of metal-siderophores across the OM (16). Unlike the ExbBD-TonB system, however, the physiological role of the Tol-Pal complex has not been elucidated, despite being discovered over four decades ago (17, 18). The Tol-Pal complex has been shown to be important for OM invagination during cell division (19), but mutations in the *tol-pal* genes also result in a variety of phenotypes, such as hypersensitivity to detergents and antibiotics, leakage of periplasmic proteins, and prolific shedding of OM vesicles, all indicative of an unstable OM (8). In addition, removing the *tol-pal* genes causes envelope stress and up-regulation of the σ^E and Rcs phosphorelay responses (20, 21). It has thus been suggested that the Tol-Pal complex may in fact be important for OM stability and biogenesis. Interestingly, the *tol-pal* genes are often found in the same operon as *ybgC* (9), which encodes an acyl thioesterase shown to interact with PL biosynthetic enzymes in *E. coli* (22). This association suggests that the Tol-Pal complex may play a role in PL metabolism and/or transport.

Here, we report that the Tol-Pal complex is important for retrograde PL transport and OM lipid homeostasis in *E. coli*. We show that cells lacking the Tol-Pal complex exhibit defects in OM lipid asymmetry, as judged by the presence of outer leaflet PLs. We further demonstrate that *tol-pal* mutants accumulate excess PLs (relative to LPS) in the OM, indicating lipid imbalance in the membrane. Finally, using OM PL turnover as readout, we establish that the Tol-Pal complex is functionally important for efficient transport of PLs from the OM back to the IM. Our work solves a longstanding question on the physiological role of the Tol-Pal complex, and provides novel mechanistic insights into lipid homeostasis in the OM.

Results

Cells lacking the Tol-Pal complex exhibit defects in OM lipid asymmetry

To elucidate the function of the Tol-Pal complex, we set out to characterize the molecular nature of OM defects observed in *tol-pal* mutants in *E. coli*. Defects in the assembly of OM components typically lead to perturbations in OM lipid asymmetry (23, 24). This is characterized by the accumulation of PLs in the outer leaflet of the OM, which serve as substrates for PagP-mediated acylation of LPS (lipid A) (25). To determine if *tol-pal* mutants exhibit defects in OM lipid asymmetry, we analyzed lipid A acylation in strains lacking any member of the Tol-Pal complex. We demonstrated that each of the mutants accumulate more hepta-acylated lipid A in the OM compared to wild-type (WT) cells (Fig. 1). This OM defect, and the resulting SDS/EDTA sensitivity in these *tol-pal* mutants, are all corrected in the complemented strains (Fig. 1 and Fig. S1). We also examined other strains with known OM permeability defects. We detected increased lipid A acylation in strains with either impaired OMP (*bamB*, *bamD*, Δ*surA*) or LPS (*lptD4213*) biogenesis, as would be expected, but not in strains lacking covalent tethering between the cell wall and the OM (Δ*lpp*) (Fig. 1). Even though the Δ*lpp* mutant is known to exhibit pleiotropic phenotypes (26, 27), it does not have perturbations in OM lipid asymmetry. In contrast to OMP or LPS assembly mutants, *tol-pal* strains produce WT levels of major OMPs and LPS in the OM (Fig. S2). These results indicate that *tol-pal* mutations lead to accumulation of PLs in the outer leaflet of the OM independent of OMP and LPS biogenesis pathways.

Cells lacking the Tol-Pal complex have disrupted OM lipid homeostasis

We hypothesized that the loss of OM lipid asymmetry in *tol-pal* mutants is due to defects in PL transport across the cell envelope. To test this, we examined the steady-state distribution of

PLs (specifically labelled with [^{3}H]-glycerol) between the IM and the OM in WT and *tol-pal* strains. We established that *tol-pal* mutants have ~1.4-1.6-fold more PLs in their OMs (relative to the IMs) than the WT strain (Fig. 2*A* and Fig. S4). To ascertain if this altered distribution of PLs between the two membranes was due to the accumulation of more PLs in the OMs of *tol-pal* mutants, we quantified the ratios of PLs to LPS (both lipids now labelled with [^{14}C]-acetate) following OM isolation and differential extraction. *tol-pal* mutants contain ~1.5-2.5-fold more PLs (relative to LPS) in their OMs, when compared to the WT strain (Fig. 2*B* and Fig. S5). Since *tol-pal* mutants produce WT LPS levels (Fig. S2*B*), we conclude that strains lacking the Tol-Pal complex accumulate excess PLs in their OMs, a phenotype that can be corrected via genetic complementation (Fig. 2). Consistent with this idea, *tol-pal* mutants, unlike WT (28), are able to survive the toxic effects of LPS overproduction (Fig. S6), possibly due to a more optimal balance of PLs to LPS in their OMs. Importantly, having excess PLs makes the OM unstable, and can account for the permeability and vesiculation phenotypes observed in *tol-pal* mutants (8, 27). Furthermore, cells lacking the Tol-Pal complex are on average shorter and wider than WT cells (when grown under conditions with no apparent division defects) (19); this reflects an increase in surface area of the rod-shaped cells, perhaps a result of increase in OM lipid content. As expected, we did not observe disruption of lipid homeostasis in the Δ*lpp* mutant (Fig. 2). However, we observed higher PL content in the OMs of strains defective in OMP assembly. We reasoned that this increase may help to stabilize the OM by filling the voids created by the decrease in properly-assembled OMPs. Since strains lacking the Tol-Pal complex have proper OMP assembly (Fig. S2*A*), the phenotype of excess PL build-up in the OM must be due to a different problem. Our results suggest that *tol-pal* mutations directly affect PL transport processes, and therefore OM lipid homeostasis.

Cells lacking the Tol-Pal complex are defective in retrograde PL transport

Unlike for other OM components, PL transport between the IM and the OM is bidirectional (5-7). Therefore, a simple explanation for the accumulation of excess PLs in the OMs of cells lacking the Tol-Pal complex is that there are defects in retrograde PL transport. To evaluate this possibility, we used the turnover of OM PLs (specifically anionic lipids, including phosphatidylserine (PS), phosphatidylglycerol (PG), and cardiolipin (CL)) as readout for the transport of PLs back to the IM (Fig. 3*A*). As an intermediate during the biosynthesis of the major lipid phosphatidylethanolamine (PE), PS is converted to PE by the PS decarboxylase (PSD) at the IM, and typically exists only at trace levels (29). PG and CL have relatively short lifetimes (30, 31). While the pathways for CL turnover are not known, PG can be converted to PE via PS (32). Since all known enzymes involved in possible pathways of converting PG to PS, and then to PE, are localized in the IM (29), the turnover of OM anionic lipids require, and therefore report on, retrograde PL transport. Such an assay has previously been employed to demonstrate retrograde transport for PS (7).

Using a strain expressing a temperature-sensitive (Ts) allele (*psd2*) of the gene encoding PSD (33), we pulse-labelled PLs with [^{32}P]-phosphate at the restrictive temperature (42˚C), and monitored the turnover of individual PL species in the OM during a chase period at the permissive temperature (30˚C). At 42˚C, the *psd2* strain accumulates substantial amounts of PS in both the IM and the OM (Fig. 3*B*, 0-min time point), as previously reported (33). With the restoration of PSD activity at 30˚C, we observed initial increase but eventual conversion of PS to PE in both membranes (Fig. 3*B*, after 45-min time point), indicating that OM PS is transported back to the IM, converted to PE, and subsequently re-equilibrated to the OM (7). We also detected higher PG/CL content in the *psd2* strain at 42˚C, and saw rapid conversion of these lipids to PE in both membranes at 30˚C (Fig. 3*B*), at rates comparable to what was previously

reported (for PG) (32). The fact that PS levels increase initially but decrease after 45 min into the chase is consistent with the idea that PS is an intermediate along the turnover pathway for PG (32), as well as for CL. To confirm this observation, we also performed the chase at 42˚C in the presence of a known PSD inhibitor (34) (these conditions completely shut down PSD activity), and found quantitative conversion of PG/CL to PS in both membranes (Fig. S7). We further showed that PG/CL-to-PE conversion is abolished in the presence of the pmf uncoupler carbonyl cyanide *m*-chlorophenyl hydrazone (CCCP)(Fig. 3*C*), demonstrating that cellular energy sources are required for this process (32), and that conversion occurs in the IM. The observation of PG/CL turnover in the IM is thus expected. The fact that we also observed the conversion of OM PG/CL to PE points towards an intact retrograde PL transport pathway for these lipids in the otherwise WT cells. Notably, turnover of OM PG/CL appears to be slightly faster than that of IM PG/CL (Fig. 3*B*), suggesting that retrograde transport of these lipids may be coupled to the turnover process.

We performed the same pulse-chase experiments with *psd2* cells lacking TolA. We detected PG/CL-to-PE conversion in the IM at rates comparable to WT (Fig. 3*D*, *F*; ~67% and ~71% PG/CL turnover at 2 h-chase in Δ*tolA* and WT IMs, respectively (Fig. 4*A*)), demonstrating that there are functional PG/CL turnover pathways in the Δ*tolA* mutant. In contrast, we observed substantial reduction of the turnover of OM PG/CL in these cells (Fig. 3*D*, *F*; ~53% PG/CL turnover at 2 h-chase in the Δ*tolA* OM, compared to ~79% for WT (Fig. 4*A*)), even though PS conversion to PE appears intact. These results indicate an apparent defect in the movement of PG and CL (but not PS) from the OM back to the IM, which is restored when complemented with functional $tolA_{WT}$ (Fig. 3*E*, *F* and Fig. 4*A*). Δ*tolR* mutant cells exhibit the same defect, and can similarly be rescued by complementation with functional $tolR_{WT}$ (Fig. 4*A*). In contrast, no rescue was observed when Δ*tolR* was complemented using a *tolR* allele with impaired ability to utilize

204 the pmf (*tolR*$_{D23R}$) (14) (Fig. 4*A* and Fig. S1); this indicates that Tol-Pal function is required for
205 efficient PG/CL transport. We also examined PG/CL turnover in *psd2* cells lacking BamB,
206 which accumulate excess PLs in the OM due to defects in OMP assembly (Fig. 2). Neither IM
207 nor OM PG/CL turnover is affected (Fig. 4*A*), highlighting the different basis for OM PL
208 accumulation in this strain compared to the *tol-pal* mutants. Our assay does not report on the
209 retrograde transport of major lipid PE, which is relatively stable (30). However, since *tol-pal*
210 mutants accumulate ~1.5-fold more PLs in the OM (Fig. 2) without gross changes in PL
211 composition (compared to WT) (Fig. S9), PE transport must also have been affected. We
212 conclude that the Tol-Pal complex is required for the retrograde transport of bulk PLs in *E. coli*.
213
214 **Overexpressing a putative PL transport system partially rescues defects in retrograde PL**
215 **transport observed in *tol-pal* mutants**
216 Removing the Tol-Pal complex does not completely abolish retrograde PG/CL transport,
217 indicating that there are other systems involved in this process. The OmpC-Mla system is
218 important for the maintenance of OM lipid asymmetry, and is proposed to do so via retrograde
219 PL transport (35, 36). To determine if this system plays a major role in retrograde PL transport in
220 cells lacking the Tol-Pal complex, we examined OM PG/CL turnover in Δ*tolA* cells also lacking
221 MlaC, the putative periplasmic lipid chaperone of the system. We first showed that cells lacking
222 MlaC alone do not exhibit defects in OM PG/CL turnover (Fig. 4*A*). Evidently, removing MlaC
223 also does not exacerbate the defects in retrograde PL transport in cells lacking the Tol-Pal
224 complex, given that overall turnover rates of IM and OM PG/CL are similarly reduced in the
225 double mutant. These results indicate that the OmpC-Mla system does not contribute
226 significantly to retrograde transport of bulk lipids when expressed at physiological levels, as has
227 been previously suggested (35). We also tested whether overexpressing the OmpC-Mla system

can restore retrograde PL transport in *tol-pal* mutants. Interestingly, overexpression of MlaC and the IM MlaFEDB complex (37), but not MlaA, partially rescues OM PG/CL turnover in the Δ*tolA* mutant (Fig. 4*B*). However, this has no consequential effect on alleviating permeability defects observed in the Δ*tolA* strain (Fig. S10), presumably because the OmpC-Mla system may have higher specificity for PG (37). Since PE is the predominant PL species in the OM (Fig. S9) (29), overexpressing the OmpC-Mla system may not effectively reduce the overall build-up of PLs caused by the loss of Tol-Pal function. Further to validating the putative PL transport function of the OmpC-Mla system, our observation here lends strong support to the notion that the Tol-Pal complex is indeed a major system for retrograde PL transport.

Discussion

Our work reveals that the Tol-Pal complex plays an important role in maintaining OM lipid homeostasis via retrograde PL transport. Removing the system causes accumulation of excess PLs (over LPS) in the OM (Fig. 2). While pathways for anterograde PL transport remain to be discovered, this result indicates that PL flux to the OM may be intrinsically higher than that of LPS. Evidently, the ability to transport high levels of PLs to the OM allows cells to compensate for the loss of OMPs due to defects in assembly (Fig. 2). Our data suggest that cells maintain an excess flux of PLs to the OM in order to offset changes in the unidirectional assembly pathways for other OM components, and then return the PL surplus to the IM via the Tol-Pal complex (and other redundant systems). Having bidirectional PL transport therefore provides a mechanism to regulate and ensure the formation of a stable OM.

It is not clear how the Tol-Pal complex may mediate retrograde PL transport. It is possible that this machine directly binds and transports lipids, although there are no obvious lipid

252 binding motifs or cavities found in available structures of the periplasmic components (38, 39).
253 The Tol-Pal complex is related to the ExbBD-TonB (14, 40), Agl-Glt (41), and Mot (14, 42)
254 systems, each of which uses pmf-energized conformational changes to generate force for the
255 uptake of metal-siderophores, for gliding motility, or to power flagella rotation, respectively. In
256 addition, both the Tol-Pal and ExbBD-TonB complexes are hijacked by toxins (such as colicins)
257 and bacteriophages to penetrate the OM (43). It is therefore also possible that the Tol-Pal
258 complex acts simply as a force generator to transport other PL-binding proteins across the
259 periplasm, or perhaps bring the OM close enough to the IM for PL transfer to occur via
260 hemifusion events. For the latter scenario, one can envision energized TolA pulling the OM
261 inwards via its interaction with Pal, which is anchored to the inner leaflet of the OM (12). While
262 it remains controversial, the formation of such "zones of adhesion", or membrane contact sites,
263 has previously been proposed (44), and in fact, was suggested to be a mechanism for retrograde
264 transport of native and foreign lipids (6).

265 That the Tol-Pal complex is involved in retrograde PL transport also has significant
266 implications for Gram-negative bacterial cell division. As part of the divisome, this system is
267 important for proper OM invagination during septum constriction (19, 45, 46). How OM
268 invagination occurs is unclear. Apart from physically tethering the IM and the OM, we propose
269 that removal of PLs from the inner leaflet of the OM by the Tol-Pal complex serves to locally
270 reduce the surface area of the inner leaflet relative to the outer leaflet (47). According to the
271 bilayer-couple model (48), this may then induce the requisite negative curvature in the OM at the
272 constriction site, thus promoting formation of the new cell poles.

273 Given the importance of the Tol-Pal complex in OM stability and bacterial cell division,
274 it would be an attractive target for small molecule inhibition. This is especially so in some
275 organisms, including the opportunistic human pathogen *Pseudomonas aeruginosa*, where the

complex is essential for growth (49, 50). The lack of understanding of the true role of the Tol-Pal complex, however, has impeded progress. We believe that our work in elucidating the physiological function of this complex will accelerate efforts in this direction, and contribute towards the development of new antibiotics in our ongoing fight against recalcitrant Gram-negative infections.

Materials and Methods

Detailed methods can be found in *SI*.

Acknowledgments

We thank Zhi-Soon Chong for constructing the Δ*mlaC* allele, and Manjula Reddy (Center for Cellular and Molecular Biology) for providing the *lpxC1272* mutant and the p*yciM* plasmid. We thank Chee-Geng Chia for performing preliminary experiments. We are grateful to Swaine Chen (NUS), Rajeev Misra (Arizona State U), and Daniel Kahne (Harvard U) for their generous gifts of α-OmpC, α-OmpF, and α-LptE and α-BamA antibodies, respectively. Finally, we thank William F. Burkholder (Institute of Molecular and Cell Biology) and Jean-Francois Collet (U Catholique de Louvain) for critical comments and suggestions on the manuscript. This work was supported by the National University of Singapore Start-up funding, the Singapore Ministry of Education Academic Research Fund Tier 1 grant, and the Singapore Ministry of Health National Medical Research Council under its Cooperative Basic Research Grant (NMRC/CBRG/0072/2014) (to S.-S.C.).

References

1. Nikaido H (2003) Molecular basis of bacterial outer membrane permeability revisited. *Microbiol Mol Biol Rev* 67(4):593-656.
2. Okuda S, Sherman DJ, Silhavy TJ, Ruiz N, Kahne D (2016) Lipopolysaccharide transport and assembly at the outer membrane: the PEZ model. *Nat Rev Microbiol* 14:337-345.
3. Hagan CL, Silhavy TJ, Kahne D (2011) β-barrel membrane protein assembly by the Bam complex. *Annu Rev Biochem* 80:189-210.
4. Okuda S, Tokuda H (2011) Lipoprotein sorting in bacteria. *Annu Rev Microbiol* 65:239-259.
5. Donohue-Rolfe AM, Schaechter M (1980) Translocation of phospholipids from the inner to the outer membrane of *Escherichia coli*. *Proc Natl Acad Sci USA* 77(4):1867-1871.
6. Jones NC, Osborn MJ (1977) Translocation of phospholipids between the outer and inner membranes of *Salmonella typhimurium*. *J Biol Chem* 252(20):7405-7412.
7. Langley KE, Hawrot E, Kennedy EP (1982) Membrane assembly: movement of phosphatidylserine between the cytoplasmic and outer membranes of *Escherichia coli*. *J Bacteriol* 152(3):1033-1041.
8. Lloubes R, et al. (2001) The Tol-Pal proteins of the *Escherichia coli* cell envelope: an energized system required for outer membrane integrity? *Res Microbiol* 152:523-529.
9. Sturgis JN (2001) Organisation and evolution of the *tol-pal* gene cluster. *J Mol Microbiol Biotechnol* 3(1):113-122.
10. Cascales E, Gavioli M, Sturgis JN, Lloubes R (2000) Proton motive force drives the interaction of the inner membrane TolA and outer membrane Pal proteins in *Escherichia coli*. *Mol Microbiol* 38(4):904-915.

11. Germon P, Ray MC, Vianney A, Lazzaroni JC (2001) Energy-dependent conformational changes in the TolA protein of *Escherichia coli* involves its N-terminal domain, TolQ, and TolR. *J Bacteriol* 183(14):4110-4114.

12. Godlewska R, Wisniewska K, Pietras Z, Jagusztyn-Krynicka EK (2009) Peptidoglycan-associated lipoprotein (Pal) of Gram-negative bacteria: function, structure, role in pathogenesis and potential application in immunoprophylaxis. *FEMS Microbiol Lett* 298:1-11.

13. Walburger A, Lazdunski C, Corda Y (2002) The Tol/Pal system function requires an interaction between the C-terminal domain of TolA and the N-terminal domain of TolB. *Mol Microbiol* 44(3):695-708.

14. Cascales E, Lloubes R, Sturgis JN (2001) The TolQ-TolR proteins energize TolA and share homologies with the flagellar motor proteins MotA-MotB. *Mol Microbiol* 42(3):795-807.

15. Witty M, et al. (2002) Structure of the periplasmic domain of *Pseudomonas aeruginosa* TolA: evidence for an evolutionary relationship with the TonB transporter protein. *EMBO J* 21(16):4207-4218.

16. Gresock MG, Kastead KA, Postle K (2015) From homodimer to heterodimer and back: elucidating the TonB energy transduction cycle. *J Bacteriol* 197(21):3433-3445.

17. Bernstein A, Rolfe B, Onodera K (1972) Pleiotropic properties and genetic organization of the *tolA, B* locus of *Escherichia coli* K-12. *J Bacteriol* 112(1):74-83.

18. Lazzaroni JC, Portalier RC (1981) Genetic and biochemical characterization of periplasmic-leaky mutants of *Escherichia coli* K-12. *J Bacteriol* 145(3):1351-1358.

19. Gerding MA, Ogata Y, Pecora ND, Niki H, de Boer PAJ (2007) The trans-envelope Tol-Pal complex is part of the cell division machinery and required for proper outer-

membrane invagination during cell constriction in *E. coli*. *Mol Microbiol* 63(4):1008-1025.

20. Vines ED, Marolda CL, Balachandran A, Valvano MA (2005) Defective O-antigen polymerization in *tolA* and *pal* mutants of *Escherichia coli* in response to extracytoplasmic stress. *J Bacteriol* 187(10):3359-3368.

21. Clavel T, Lazzaroni JC, Vianney A, Portalier R (1996) Expression of the *tolQRA* genes of *Escherichia coli* K-12 is controlled by the RcsC sensor protein involved in capsule synthesis. *Mol Microbiol* 19(1):19-25.

22. Gully D, Bouveret E (2006) A protein network for phospholipid synthesis uncovered by a variant of the tandem affinity purification method in *Escherichia coli*. *Proteomics* 6:282-293.

23. Wu T, et al. (2006) Identification of a protein complex that assembles lipopolysaccharide in the outer membrane of *Escherichia coli*. *Proc Natl Acad Sci USA* 103(31):11754-11759.

24. Ruiz N, Gronenberg LS, Kahne D, Silhavy TJ (2008) Identification of two inner-membrane proteins required for the transport of lipopolysaccharide to the outer membrane of *Escherichia coli*. *Proc Natl Acad Sci USA* 105(14):5537-5542.

25. Bishop RE (2005) The lipid A palmitoyltransferase PagP: molecular mechanisms and role in bacterial pathogenesis. *Mol Microbiol* 57(4):900-912.

26. Yem DW, Wu HC (1978) Physiological characterization of an *Escherichia coli* mutant altered in the structure of murein lipoprotein. *J Bacteriol* 133(3):1419-1426.

27. Bernadac A, Gavioli M, Lazzaroni JC, Raina S, Lloubes R (1998) *Escherichia coli tol-pal* mutants form outer membrane vesicles. *J Bacteriol* 180(18):4872-4878.

369 28. Fuhrer F, Langklotz S, Narberhaus F (2006) The C-terminal end of LpxC is required for
370 degradation by the FtsH protease. *Mol Microbiol* 59(3):1025-1036.
371 29. Cronan JE (2003) Bacterial membrane lipids: where do we stand? *Annu Rev Microbiol*
372 57:203-224.
373 30. Kanfer J, Kennedy EP (1963) Metabolism and function of bacterial lipids I. Metabolism
374 of phospholipids in *Escherichia coli* B. *J Biol Chem* 238(9):2919-2922.
375 31. Kanemasa Y, Akamatsu Y, Nojima S (1967) Composition and turnover of the
376 phospholipids in *Escherichia coli*. *Biochim Biophys Acta* 144:382-390.
377 32. Yokoto K, Kito M (1982) Transfer of the phosphatidyl moiety of phosphatidylglycerol to
378 phosphatidylethanolamine in *Escherichia coli*. *J Bacteriol* 151(2):952-961.
379 33. Hawrot E, Kennedy EP (1978) Phospholipid composition and membrane function in
380 phosphatidylserine decarboxylase mutants of *Escherichia coli*. *J Biol Chem*
381 253(22):8213-8220.
382 34. Satre M, Kennedy EP (1978) Identification of bound pyruvate essential for the activity of
383 phosphatidylserine decarboxylase of *Escherichia coli*. *J Biol Chem* 253(2):479-483.
384 35. Malinverni JC, Silhavy TJ (2009) An ABC transport system that maintains lipid
385 asymmetry in the Gram-negative outer membrane. *Proc Natl Acad Sci USA*
386 106(19):8009-8014.
387 36. Chong ZS, Woo WF, Chng SS (2015) Osmoporin OmpC forms a complex with MlaA to
388 maintain outer membrane lipid asymmetry in *Escherichia coli*. *Mol Microbiol*
389 98(6):1133-1146.
390 37. Thong S, et al. (2016) Defining key roles for auxillary proteins in an ABC transporter
391 that maintains bacterial outer membrane lipid asymmetry. *eLife* 5:e19042.

392 38. Deprez C, et al. (2005) Solution structure of the *E. coli* TolA C-termical domain reveals
393 conformational changes upon binding to the phage g3p N-terminal domain. *J Mol Biol*
394 346(4):1047-1057.
395 39. Carr S, Penfold CN, Bamford V, James R, Hemmings AM (2000) The structure of TolB,
396 an essential component of the *tol*-dependent translocation system, and its protein-protein
397 interaction with the translocation domain of colicin E9. *Structure* 8(1):57-66.
398 40. Celia H, et al. (2016) Structural insight into the role of the Ton complex in energy
399 transduction. *Nature* 538(7623):60-65.
400 41. Faure LM, et al. (2016) The mechanism of force transmission at bacterial focal adhesion
401 complexes. *Nature* 539(7630):530-535.
402 42. Thormann KM, Paulick A (2010) Tuning the flagellar motor. *Microbiology* 156(Pt
403 5):1275-1283.
404 43. Cascales E, et al. (2007) Colicin biology. *Microbiol Mol Biol Rev* 71(1):158-229.
405 44. Bayer ME (1991) Zones of membrane adhesion in the cryofixed envelope of *Escherichia*
406 *coli*. *J Struct Biol* 107(3):268-280.
407 45. Yeh YC, Comolli LR, Downing KH, Shapiro L, McAdams HH (2010) The *Caulobacter*
408 Tol-Pal complex is essential for outer membrane integrity and the positioning of a polar
409 localization factor. *J Bacteriol* 192(19):4847-4858.
410 46. Jacquier N, Frandi A, Viollier PH, Greub G (2015) Disassembly of a medial
411 transenvelope structure by antibiotics during intracellular division. *Chem Biol*
412 22(9):1217-1227.
413 47. McMahon HT, Gallop JL (2005) Membrane curvature and mechanisms of dynamic cell
414 membrane remodelling. *Nature* 438(7068):590-596.

415 48. Sheetz MP, Singer SJ (1974) Biological membranes as bilayer couples. A molecular
416 mechanism of drug-erythrocyte interactions. *Proc Natl Acad Sci USA* 71(11):4457-4461.
417 49. Dennis JJ, Lafontaine ER, Sokol PA (1996) Identification and characterization of the
418 *tolQRA* genes of *Pseudomonas aeruginosa*. *J Bacteriol* 178(24):7059-7068.
419 50. Lo Sciuto A, et al. (2014) The periplasmic protein TolB as a potential drug target in
420 *Pseudomonas aeruginosa*. *PLoS One* 9:e103784.
421 51. Casadaban MJ (1976) Transposition and fusion of the *lac* genes to selected promoters
422 in *Escherichia coli* using bacteriophage lambda and Mu. *J Mol Biol* 104:541-555.
423 52. Datsenko KA, Wanner BL (2000) One-step inactivation of chromosomal genes in
424 *Escherichia coli* K-12 using PCR products. *Proc Natl Acad Sci USA* 97():6640-6645.
425 53. Baba T, et al. (2006) Construction of *Escherichia coli* K-12 in-frame, single-gene
426 knockout mutants: the Keio collection. *Mol Syst Biol* 2:2006.0008.
427 54. Silhavy TJ, Berman ML, Enquist LW (1984) *Experiments with Gene fusions* (Cold
428 Spring Harbor Laboratory Press, Cold Spring Harbor, New York).
429 55. Zhou Z, Lin S, Cotter RJ, Raetz CRH (1999) Lipid A modifications characteristic of
430 *Salmonella typhimurium* are induced by NH_4VO_3 in *Escherichia coli* K-12. *J Biol Chem*
431 274():18503-18514.
432 56. Chng SS, Gronenberg LS, Kahne D (2010) Proteins required for lipopolysaccharide
433 transport in *Escherichia coli* form a transenvelope complex. *Biochemistry* 49:4565-4567.
434 57. Laemmli UK (1970) Cleavage of structural proteins during the assembly of the head of
435 bacteriophage T4. *Nature* 227:680-685.

436 58. Khetrapal V, et al. (2015) A set of powerful negative selection systems for unmodified
437 Enterobacteriaceae. *Nucleic Acids Res* 43:e83.

438 59. Charlson ES, Werner JN, Misra R (2006) Differential effects of *yfgL* mutation on
439 *Escherichia coli* outer membrane proteins and lipopolysaccharide. *J Bacteriol* 188:7186-
440 7194.

441 60. Mahalakshmi S, Sunayana MR, SaiSree L, Reddy M (2014) *yciM* is an essential gene
442 required for regulation of lipopolysaccharide synthesis in *Escherichia coli*. *Mol*
443 *Microbiol* 91:145-157.

444 61. Ruiz N, Chng SS, Hinikera A, Kahne D, Silhavy TJ (2010) Nonconsecutive disulphide
445 bond formation in an essential integral outer membrane protein. *Proc Natl Acad Sci USA*
446 107:12245-12250.

447 62. Ruiz N, Falcone B, Kahne D, Silhavy TJ (2005) Chemical conditionality: a genetic
448 strategy to probe organelle assembly. *Cell* 121:307-317.

449 63. Wu T, et al. (2005) Identification of a multicomponent complex required for outer
450 membrane biogenesis in *Escherichia coli*. *Cell* 121:235-245.

451 64. Guzman LM, Belin D, Carson MJ, Beckwith J (1995) Tight regulation, modulation, and
452 high-level expression by vectors containing the arabinose P_{BAD} promoter. *J Bacteriol*
453 177:4121-4130.

454 65. Dalebroux ZD, Matamouros S, Whittington D, Bishop RE, Miller SI (2014) PhoPQ
455 regulates acidic glycerophospholipid content of the *Salmonella typhimurium* outer
456 membrane. *Proc Natl Acad Sci USA* 111:1963-1968.

Figure Legends

Fig. 1. Cells lacking the Tol-Pal complex accumulate PLs in the outer leaflet of the OM as judged by lipid A acylation. Thin layer chromatographic (TLC) analysis of [^{32}P]-labelled lipid A extracted from WT, Δ*tol-pal*, and various mutant strains (*see text*). Where indicated, WT and *tol-pal* mutants contain an empty pET23/42 plasmid (p) (23) or one expressing the corresponding *tol-pal* gene(s) at low levels (e.g. p*tol-pal*). As a positive control for lipid A acylation, WT cells were treated with EDTA (to chelate Mg^{2+} and destabilize the LPS layer) prior to extraction. Equal amounts of radioactivity were spotted for each sample. Lipid spots annotated # represent 1-pyrophosphoryl-lipid A. Average percentages of lipid A acylation and standard deviations were quantified from triplicate experiments and plotted below. Student's t-tests: * $p < 0.005$ as compared to WT.

Fig. 2. Cells lacking the Tol-Pal complex accumulate excess PLs (relative to LPS) in the OM. (*A*) Steady-state distribution of [^{3}H]-glycerol labelled PLs between the IM and the OM of WT, Δ*tol-pal*, and various mutant strains (*upper panel*). Distribution of [^{3}H]-labelled PLs in the OMs of respective mutants expressed as fold changes relative to the WT OM (*lower panel*). The IMs and OMs from both WT and *tol-pal* mutants were separated with equal efficiencies during sucrose density gradient fractionation (Fig. S3). (*B*) Steady-state PL:LPS ratios in the OMs of WT, Δ*tol-pal*, and various mutant strains (*upper panel*). Lipids were labelled with [^{14}C]-acetate and differentially extracted from OMs (Fig. S5). OM PL:LPS ratios of respective mutants expressed as fold changes relative to that in the WT OM (*lower panel*). Error bars represent standard deviations calculated from triplicate experiments. Student's t-tests: * $p < 0.05$; ** $p < 0.005$; NS, not significant (as compared to WT).

Fig. 3. Cells lacking the Tol-Pal complex are defective in OM PG/CL turnover. (*A*) A schematic diagram depicting movement and turnover of PE, PG and CL (major), and PS (trace) in the cell envelope. (*B*-*E*) TLC time-course analyses of [^{32}P]-pulse-labelled PLs extracted from the IMs and OMs of (*B*) WT, (*C*) WT (with CCCP added), (*D*) Δ*tolA*, and (*E*) *tolA*-complemented strains also harboring the *psd2* mutation. The average percentage levels of PE, PG/CL, and PS in the IM and OM at each time point, together with standard deviations, were quantified from triplicate experiments and shown on the right. (*F*) The percentage levels of PG/CL in the IMs and OMs from (*B*-*E*) normalized to the corresponding levels at the start of the chase (0 min).

Fig. 4. Tol-Pal function is required for efficient retrograde PG/CL transport, as judged by OM PG/CL turnover rates. Single time-point (2-h chase) quantification of the turnover rate of [^{32}P]-labelled PG/CL in the IMs and OMs of (*A*) WT, *tol-pal* and various mutant strains, and (*B*) Δ*tolA* overexpressing OmpC-Mla components, all in the *psd2* background (*see text*) (Fig. S8). Percentage PG/CL turnover at 2-h is expressed as $[(\%PG/CL)_{start} - (\%PG/CL)_{2h}]/[(\%PG/CL)_{start}]$. Average percentage lipid levels and standard deviations were quantified from triplicate experiments. Student's t-tests: * $p < 0.0005$ as compared to WT; ** $p < 0.0005$ as compared to Δ*tolA*.

Figures

Figure 1

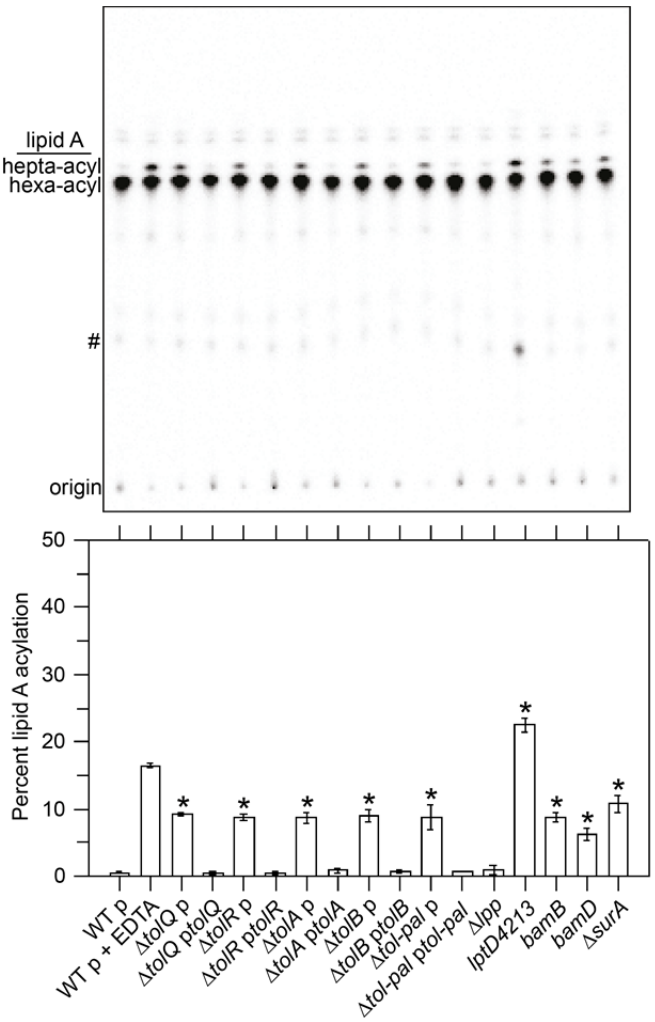

505 **Figure 2**

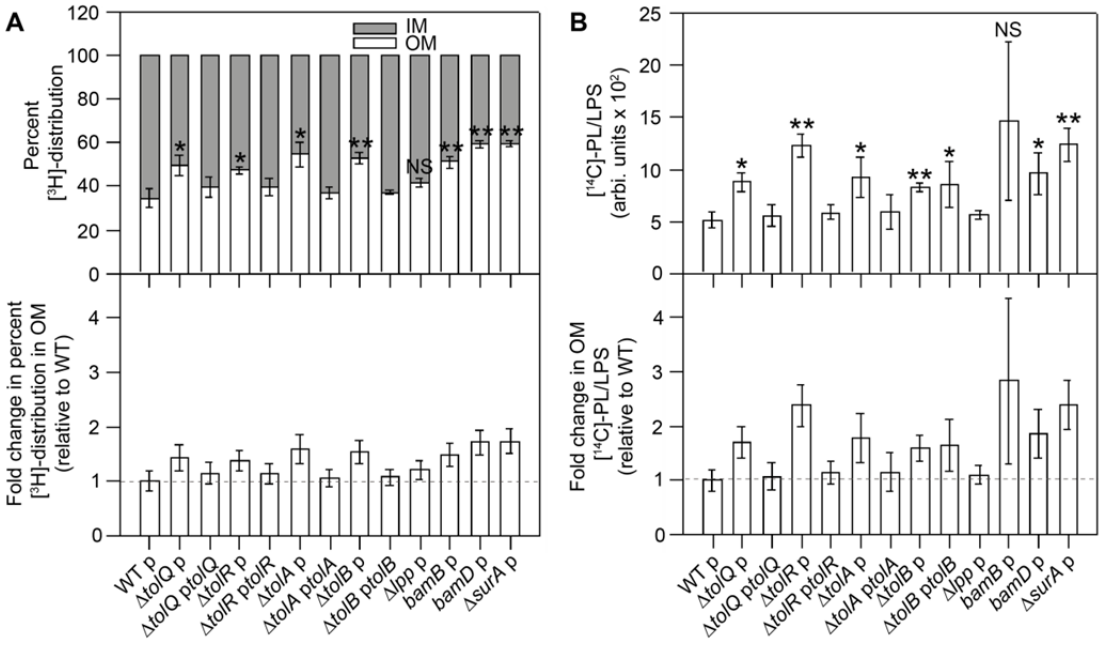

506

507

Figure 3

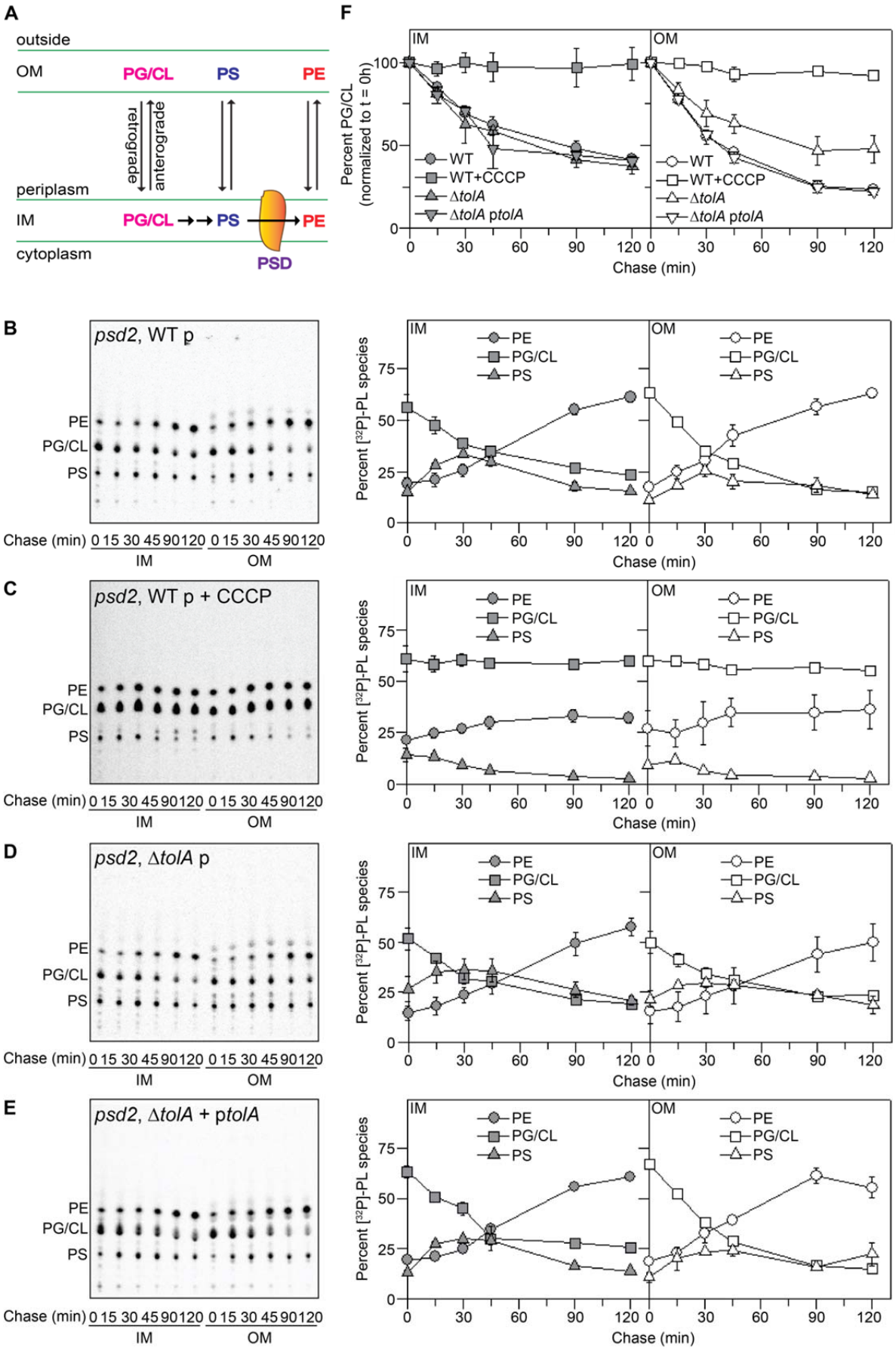

509 **Figure 4**

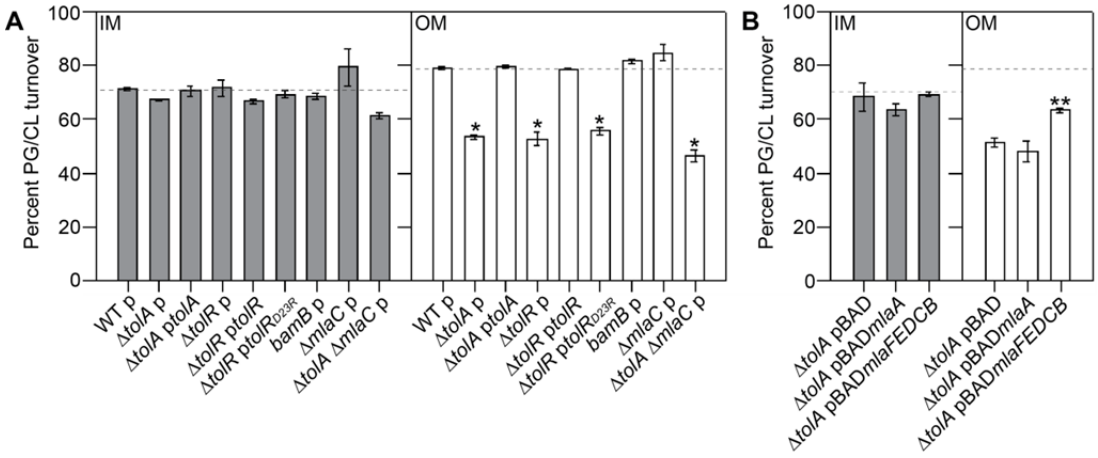

510

Supporting Information

Title: A trans-envelope complex maintains outer membrane lipid homeostasis via retrograde phospholipid transport in *Escherichia coli*

Authors: Rahul Shrivastava[a], Xiang'Er Jiang[b], Shu-Sin Chng[a,b*]

Affiliations:

[a]Department of Chemistry, National University of Singapore, Singapore 117543.

[b]Singapore Center for Environmental Life Sciences Engineering, National University of Singapore (SCELSE-NUS), Singapore 117456.

*To whom correspondence should be addressed. E-mail: chmchngs@nus.edu.sg

Materials and Methods

Bacterial strains and growth conditions

All the strains used in this study are listed in Table S1. *Escherichia coli* strain MC4100 [*F⁻ araD139 Δ(argF-lac) U169 rpsL150 relA1 flbB5301 ptsF25 deoC1 ptsF25 thi*] (51) was used as the wild-type (WT) strain for most of the experiments. To achieve accumulation of phosphatidylserine (PS) in cells, a temperature-sensitive phosphatidylserine decarboxylase mutant (*psd2*), which accumulates PS at the non-permissive temperature, was used (33). NR754, an *araD*$^{+}$ revertant of MC4100 (24), was used as the WT strain for experiments involving overexpression of *lpxC* from the arabinose-inducible promoter (P_{BAD}). Δ*tolQ*, Δ*tolA* and Δ*tol-pal* deletions were constructed using recombineering (52) and all other gene deletion strains were obtained from the Keio collection (53). Whenever needed, the antibiotic resistance cassettes were flipped out as described (52). Gene deletion cassettes were transduced into relevant genetic background strains via P1 transduction (54). Luria-Bertani (LB) broth (1% tryptone and 0.5% yeast extract, supplemented with 1% NaCl) and agar were prepared as previously described (54). Strains were grown in LB medium with shaking at 220 rpm at either 30˚C, 37˚C, or 42˚C, as indicated. When appropriate, kanamycin (Kan; 25 μg ml^{-1}), chloramphenicol (Cam; 30 μg ml^{-1}) and ampicillin (Amp; 125 μg ml^{-1}) were added.

Plasmid construction

All the plasmids used in this study are listed in Table S2. Desired genes were amplified from MC4100 chromosomal DNA using the indicated primers (sequences in Table S3). Amplified products were digested with indicated restriction enzymes (New England Biolabs),

which were also used to digest the carrying vector. After ligation, recombinant plasmids were transformed into competent NovaBlue (Novagen) cells and selected on LB plates containing appropriate antibiotics. DNA sequencing (Axil Scientific, Singapore) was used to verify the sequence of the cloned gene.

To generate *tolR*$_{D23R}$ mutant construct, site-directed mutagenesis was conducted using relevant primers listed in Table S3 with pET23/42*tolR* as the initial template. Briefly, the entire template was amplified by PCR and the resulting PCR product mixture digested with DpnI for > 1 h at 37˚C. Competent NovaBlue cells were transformed with 1 µl of the digested PCR product and plated onto LB plates containing ampicillin. DNA sequencing (Axil Scientific, Singapore) was used to verify the introduction of the desired mutation.

Analysis of [^{32}P]-labelled lipid A

Mild acid hydrolysis was used to isolate lipid A as previously described (55) with some modifications. 5-ml cultures were grown in LB broth (inoculated from an overnight culture at 1:100 dilution) containing [^{32}P]-disodium phosphate (final 1 µCi ml^{-1}; Perkin Elmer product no. NEX011001MC) till mid-log phase (OD600 ~0.5 - 0.7). One MC4100 WT culture labelled with [^{32}P] was treated with EDTA (25 mM pH 8.0) for 10 min prior to harvesting. Cells were harvested at 4,700 x *g* for 10 min, washed twice with 1 ml PBS (137 mM NaCl, 2.7 mM KCl, 10 mM Na_2HPO_4, 1.8 mM KH_2PO_4, pH 7.4) and suspended in PBS (0.32 ml) again. Chloroform (0.4 ml) and methanol (0.8 ml) were added and the mixtures were incubated at room temperature for 20 min with slow shaking (60 rpm) to make the one-phase Bligh-Dyer mixture (chloroform:methanol:water = 1:2:0.8). Mixtures were then centrifuged at 21,000 x *g* for 30 min. Pellets obtained were washed once with fresh one-phase Bligh-Dyer system (1 ml) and

centrifuged as above. Resulting pellets were suspended in 0.45 ml of sodium acetate (12.5 mM, pH 4.5) containing SDS (1 %) and heated at 100˚C for 30 min. After cooling to room temperature, chloroform and methanol (0.5 ml each) were added to create a two-phase Bligh-Dyer mixture (chloroform:methanol:water = 2:2:1.8). The lower (organic) phase of each mixture was collected after phase partitioning via centrifugation at 21,000 x *g* for 30 min. This was washed once with upper phase (0.5 ml) of freshly prepared two-phase Bligh-Dyer mixture and centrifuged as above. Finally, all the collected lower phases containing [^{32}P]-labelled lipid A were air-dried overnight. Dried radiolabelled lipid A samples were suspended in 50 µl of chloroform:methanol (2:1) and equal amounts (~1,000 cpm) of radioactivity were spotted on silica-gel coated TLC (Thin Layer Chromatography) plates (Merck). TLCs were developed in chambers pre-equilibrated overnight with solvent system chloroform:pyridine:98 % formic acid:water (50:50:14.6:5). TLC plates were air-dried overnight and later visualized by phosphor imaging (STORM, GE healthcare). The densitometric analysis of the spots obtained on the phosphor images of TLCs was carried out using ImageQuant TL analysis software (version 7.0, GE Healthcare). Average levels of hepta-acylated lipid A (expressed as a percentage of total lipid A in each sample) were obtained from three independent experiments.

Sucrose density gradient fractionation

Sucrose density gradient centrifugation was performed as previously described (56) with some modifications. For each strain, a 10/50-ml culture (inoculated from an overnight culture at 1:100 dilution) was grown in LB broth until OD_{600} reached ~0.5 – 0.7. For radiolabeling, indicated radioisotopes were added from the start of inoculation. Cells were harvested by centrifugation at 4,700 x *g* for 10 min, suspended to wash once in 5 ml of cold Buffer A (Tris-

HCl, 10 mM pH 8.0), and centrifuged as above. Cells were resuspended in 6 ml of Buffer B (Tris-HCl, 10 mM pH 8.0 containing 20% sucrose (w/w), 1 mM PMSF and 50 μg ml $^{-1}$ DNase I), and lysed by a single passage through a high pressure French press (French Press G-M, Glen Mills) homogenizer at 8,000 psi. Under these conditions, lipid mixing between inner and outer membranes is minimal (56). Unbroken cells were removed by centrifugation at 4,700 x *g* for 10 min. The cell lysate was collected, and 5.5 ml of cell lysate was layered on top of a two-step sucrose gradient consisting of 40% sucrose solution (5 ml) layered on top of 65% sucrose solution (1.5 ml) at the bottom of the tube. All sucrose (w/w) solutions were prepared in Buffer A. Samples were centrifuged at 39,000 rpm for 16 h in a Beckman SW41 rotor in an ultracentrifuge (Model XL-90, Beckman). 0.8-ml fractions (usually 15 fractions) were manually collected from the top of each tube.

Analysis of OMP and LPS levels in isolated OMs

OM fragments were isolated from 50 ml of cells following growth, cell lysis and application of sucrose density gradient fractionation, as described above. Instead of manual fractionation, OM fragments (~1 ml) were isolated from the 40%/65% sucrose solution interface by puncturing the side of the tube with a syringe. Buffer A (1 ml) was added to the OM fragments to lower the sucrose concentration and reduce viscosity. The OM fragments were then pelleted in a microcentrifuge at 21,000 x *g* for 30 min and then resuspended in 200 - 250 μl Buffer A. Protein concentrations of these OM preparations were determined using Bio-Rad D_C protein assay. The same amount of OM (based on protein content) for each strain was analyzed by reducing SDS-PAGE and immunoblotted using antibodies directed against OmpC, OmpF, LamB, BamA, LptE and LPS.

107

108 Analysis of steady-state [^{3}H]-glycerol-labelled PL distribution in IMs and OMs

109 To specifically label cellular PLs, 10-ml cells were grown at 37˚C in LB broth
110 (inoculated from an overnight culture at 1:100 dilution) containing [2-^{3}H]-glycerol (final 1 µCi
111 ml^{-1}; Perkin Elmer product no. NET022L001MC) until OD_{600} reached ~0.5 - 0.7. Once the
112 desired OD_{600} was achieved, cultures were immediately mixed with ice-cold Buffer A containing
113 CCCP (50 µM) to stop the labeling of the cultures. Cells were pelleted, lysed, and fractionated
114 on sucrose density gradients, as described above. 0.8-ml fractions were collected from each tube,
115 as described above, and 300 µl from each fraction was mixed with 2 ml of Ultima Gold
116 scintillation fluid (Perkin Elmer, Singapore). Radioactivity ([^{3}H]-count) was measured on a
117 scintillation counter (MicroBeta$^{2®}$, Perkin-Elmer). Based on [^{3}H]-profiles, IM and OM peaks
118 were identified and peak areas determined after background subtraction (average count of first 5
119 fractions was taken as background). For each strain, relative [^{3}H]-PL levels in the IM and OM
120 were expressed as a percentage of the sum in both membranes (see Fig. 2*A* upper panel). The
121 average percent [^{3}H]-PL in the OM for each strain (obtained from three independent
122 experiments) was then compared to that for the WT strain to calculate fold changes (see Fig. 2*A*
123 lower panel).

124

125 Determination of PL/LPS ratios in [^{14}C]-acetate labelled OMs (see Fig. S5 for workflow and
126 results)

127 To specifically label all cellular lipids (including LPS), 10-ml cells were grown at 37˚C
128 in LB broth (inoculated from an overnight culture at 1:100 dilution) containing [1-^{14}C]-acetate
129 (final 0.2 µCi ml^{-1}; Perkin Elmer product no. NEC084A001MC) until OD_{600} reached ~0.5 – 0.7.

130 At this OD, cultures were transferred immediately to ice-cold Buffer A (5 ml), pelleted, lysed,
131 and fractionated on sucrose density gradients, as described above. 0.8-ml fractions were
132 collected from each tube, as described above, and 50 µl from each fraction was mixed with 2 ml
133 of Ultima Gold scintillation fluid (Perkin Elmer, Singapore). Based on [^{14}C]-profiles, IM and
134 OM peaks were identified. OM fractions were then pooled, and treated as outlined below to
135 differentially extract PLs and LPS for relative quantification within each OM pool. For each
136 strain, the whole experiment was conducted and the OM PL/LPS ratio obtained three times.

137 Each OM pool (0.32 ml) was mixed with chloroform (0.4 ml) and methanol (0.8 ml) to
138 make a one-phase Bligh-Dyer mixture (chloroform:methanol:water = 1:2:0.8). The mixtures
139 were vortexed for 2 min and later incubated at room temperature for 20 min with slow shaking at
140 60 rpm. After centrifugation at 21,000 x *g* for 30 min, the supernatants (S1) were collected. The
141 resulting pellets (P1) were washed once with fresh 0.95 ml one-phase Bligh-Dyer solution and
142 centrifuged as above. The insoluble pellets (P2) were air dried and used for LPS quantification
143 (see below). The supernatants obtained in this step (S2) were combined with S1 to get the
144 combined supernatants (S3), which contained radiolabelled PLs. To these, chloroform (0.65 ml)
145 and methanol (0.65 ml) were added to convert them to two-phase Bligh-Dyer mixtures
146 (chloroform:methanol:water = 2:2:1.8). After a brief vortexing step, the mixtures were
147 centrifuged at 3000 x *g* for 10 min to separate the immiscible phases, and the lower organic
148 phases were collected. These were washed once with equal volumes of water and centrifuged as
149 above, and the lower organic phases (containing radiolabelled PLs) recollected and air dried.
150 Finally, the dried PLs were dissolved in 50 µl of a mixture of chloroform:methanol (2:1). Equal
151 volumes (20 µl) of PL solutions were mixed with 2 ml of Ultima Gold scintillation fluid (Perkin

Elmer, Singapore). The [^{14}C]-counts were measured using scintillation counting (MicroBeta$^{2®}$, Perkin-Elmer) and taken as the levels of PLs isolated from the OMs.

To quantify LPS, the P2 pellets were suspended in 2X reducing SDS-PAGE loading buffer (40 µl) and boiled for 10 min. Equal volumes (15 µl) were loaded and subjected to SDS-PAGE (15% Tris.HCl). Gels were air-dried between porous films (Invitrogen) and exposed to the same phosphor screen along with standards (GE healthcare). To generate a standard curve for LPS quantification, the WT OM pellet sample was serially diluted two-fold and equal volumes of diluted samples were resolved on SDS-PAGE and dried as above. The densitometric analysis of bands (i.e. LPS from each OM) was carried out using ImageQuant TL analysis software (version 7.0, GE Healthcare). To allow proper comparison and quantification, the LPS gels from triplicate experiments were exposed on the same phosphor screen along with the standards (see Fig. S5)

For each strain, the arbitrary PL/LPS ratio in the OM was obtained by taking the levels of PLs (represented by [^{14}C]-counts of PL fraction) divided by the LPS levels (represented by gel band density), averaged across three independent replicates (see Fig. S5*B*, Fig. 2*B* upper panel). The average PL/LPS ratio in the OM for each strain was then compared to that for the WT strain to calculate fold changes (see Fig. 2*B* lower panel).

<u>Phosphatidylglycerol/Cardiolipin turnover assay (pulse-chase and single time-point (2-h) analysis)</u>

PG/CL turnover pulse-chase experiments were performed using the *psd2* background, which accumulated PS and PG/CL during growth at restrictive temperature. For each strain, cells were grown in 70 ml LB broth (inoculated from an overnight culture at 1:100 dilution) at the

permissive temperature (30˚C) until OD_{600} reached ~0.15 - 0.2. The culture was then shifted for 4 h at the restrictive temperature (42˚C) and labelled with [^{32}P]-disodium phosphate (final 1 µCi ml^{-1}) during the last 30 min at the restrictive temperature (42˚C). After labeling, cells were harvested by centrifugation at 4,700 x *g* for 10 min, washed once with cold LB broth (10 ml) and centrifuged again at 4,700 x *g* for 10 min. Cells were then resuspended in fresh LB broth (70 ml) and the chase was started in the presence of non-radioactive disodium phosphate (1000-fold molar excess) at either the permissive temperature, with or without addition of carbonyl cyanide *m*-chlorophenyl hydrazone (CCCP; 50 µM), or at the restrictive temperature in the presence of hydroxylamine (HA; 10 mM). At the start (0 min) and different times (15, 30, 45, 90 and 120 min) during the chase, a portion of the culture (either 15 ml or 10 ml) was collected and mixed immediately with equal volume of ice-cold Buffer A containing CCCP (50 µM) and hydroxylamine (10 mM). Cells were harvested by centrifugation at 4,700 x *g* for 10 min and then resuspended in 6 ml of Buffer B containing CCCP (50 µM) and hydroxylamine (10 mM). Cells were lysed, and fractionated on sucrose density gradients, as described above. 0.8-ml fractions were collected from each tube, as described above. Fractions 7-9 and 12-14 contained the IM and OM fractions, respectively. To extract PLs from the IM and OM pools (2.4 ml), methanol (6 ml) and chloroform (3 ml) were added to make one-phase Bligh-Dyer mixtures. These were incubated at room temperature for 60 min with intermittent vortexing. Chloroform (3 ml) and sterile water (3 ml) were then added to generate two-phase Bligh-Dyer mixtures. After brief vortexing, the lower organic phases were separated from the top aqueous phases by centrifugation at 3,000 x *g* for 10 min. These were washed once with equal volumes of water and centrifuged as above, and the lower organic phases (containing radiolabelled PLs) recollected and air dried. Finally, the dried PLs were dissolved in 40 µl of a mixture of chloroform:methanol

(2:1) and spotted onto silica-gel coated TLC plates (Merck). Equal amounts (in cpm) of radioactivity were spotted for each sample. TLCs were developed in pre-equilibrated chambers containing solvent system chloroform:methanol:water (65:25:4). TLC plates were dried, and visualized by phosphor imaging (STORM, GE healthcare). Densitometric analysis of the PL spots on the phosphor image of TLCs was conducted using the ImageQuant TL analysis software (version 7.0, GE Healthcare). The levels of each major PL species were expressed as a percentage of all detected PL species (essentially the whole lane), and plotted against time (see Figs. 3*B*-*E* and Fig. S7).

For single time-point analysis, 30-ml cultures were grown and labelled with [^{32}P]-disodium phosphate (final 1 μCi ml^{-1}) at the restrictive temperature. For strains harboring plasmids used for overexpressing OmpC-Mla components, arabinose (0.2 %) was added during growth at the permissive as well as restrictive temperatures. After washing and resuspension in fresh LB broth (30 ml), the chase was started in the presence of non-radioactive disodium phosphate (1000-fold molar excess) at the permissive temperature. At start (0 h) and 2 h during the chase, a portion of the culture (15 and 10 ml) was collected and processed similarly as pulse chase analysis described above. The levels of PG/CL in the membranes at each time point were expressed as a percentage of the sum of PE, PS and PG/CL. For each strain, IM and OM PG/CL turnover were expressed as the difference between percentage PG/CL levels at 0-h and 2-h time points divided by that at 0-h. Average PG/CL turnover values were obtained from three independent experiments conducted (see Fig. 4 and Fig. S8).

220 OM permeability assay

221 OM sensitivity against SDS/EDTA was judged by colony-forming unit (cfu) analyses on
222 LB agar plates containing indicated concentrations of SDS/EDTA. Briefly, 5-ml cultures were
223 grown (inoculated with overnight cultures at 1:100 dilution) in LB broth at 37˚C until OD_{600}
224 reached ~1.0. Cells were normalized according to OD_{600}, first diluted to OD_{600} = 0.1 (~10^8 cells),
225 and then serial diluted in LB with seven 10-fold dilutions using 96-well microtiter plates
226 (Corning). Two microliters of the diluted cultures were manually spotted onto the plates and
227 incubated overnight at 37˚C.

228

229 LpxC overexpression (growth curves and viability assay)

230 For each strain, a 10-ml culture was inoculated in LB broth supplemented with arabinose
231 (0.2 %) from the overnight culture to make the initial OD_{600} of 0.05. Cells were grown at 37˚C
232 and the OD_{600} of the cultures was measured hourly. At the start of growth (0 h) and at 4 and 7 h
233 during growth, 100 µl of cells were collected and then serial diluted in LB/cam with six 10-fold
234 dilutions using 96-well microtiter plates (Corning). Five microliters of the non-diluted and
235 diluted cultures were manually spotted on LB/cam agar plates (no arabinose). Plates were
236 incubated overnight at 37˚C.

237

238 IM (NADH activity) and OM marker (LPS) analysis during sucrose gradient fractionation

239 The inner membrane enzyme, NADH oxidase, was used as a marker for the IM; its
240 activity was measured as previously described (56). Briefly, 30 µl of each fraction from the
241 sucrose density gradient was diluted 4-fold with 20 mM Tris.HCl, pH 8.0 in a 96-well format
242 and 120 µl of 100 mM Tris.HCl, pH 8.0 containing 0.64 mM NADH (Sigma) and 0.4 mM

dithiothreitol (DTT, Sigma) was added. Changes in fluorescence over time due to changes in NADH (λex = 340 nm, λem = 465 nm) concentration was monitored using a plate reader (Perkin Elmer). The activity of NADH oxidase in pooled IM and OM fractions relative to the sum of these fractions was determined.

LPS was used as a marker for the OM and detected using LPS dot blots. OM fractions were pooled together and 2 µl of the fractions were spotted on nitrocellulose membranes (Bio-Rad). Spotted membranes were allowed to dry at room temperature for 1 h and then the membranes were probed with antibodies against LPS.

SDS-PAGE and immunoblotting

All samples subjected to SDS-PAGE were mixed with 2X Laemmli reducing buffer and boiled for 10 min at 100˚C. Equal volumes of the samples were loaded onto the gels. Unless otherwise stated, SDS-PAGE was performed according to Laemmli using the 12% or 15% Tris.HCl gels (57). Immunoblotting was performed by transferring protein bands from the gels onto polyvinylidene fluoride (PVDF) membranes (Immun-Blot® 0.2 µm, Bio-Rad) using the semi-dry electroblotting system (Trans-Blot® TurboTM Transfer System, Bio-Rad). Membranes were blocked using 1X casein blocking buffer (Sigma). Mouse monoclonal α-OmpC antibody was a gift from Swaine Chen and used at a dilution of 1:5,000 (58). Rabbit α-LptE (from Daniel Kahne) (56) and α-OmpF antisera (Rajeev Misra) (59) were used at 1:5,000 dilutions. Rabbit α-BamA antisera (from Daniel Kahne) was used at 1:40,000 dilution. Mouse monoclonal α-LPS antibody (against LPS-core) was purchased from Hycult biotechnology and used at 1:5,000 dilutions. Rabbit polyclonal α-LamB antibodies was purchased from Bioss (USA) and used at 1:1,000 dilution. α-mouse IgG secondary antibody conjugated to HRP (from sheep) and α-rabbit

IgG secondary antibody conjugated to HRP (from donkey) were purchased from GE Healthcare and used at 1:5,000 dilutions. Luminata Forte Western HRP Substrate (Merck Milipore) was used to develop the membranes and chemiluminescent signals were visualized by G:BOX Chemi XT 4 (Genesys version1.3.4.0, Syngene).

Supplementary Figure Legends

Fig. S1. SDS/EDTA sensitivity in *tol-pal* strains can be rescued only by expressing the corresponding functional *tol-pal* gene(s) from the pET23/42 plasmid (23). Serial dilutions of cultures of wild-type (WT) and indicated *tol-pal* strains harboring pET23/42 empty vector (p), or pET23/42 encoding (*A*) functional or (*B*) non-functional *tol-pal* gene(s) (e.g. p*tolA*), were spotted on LB agar plates containing 125 μg ml^{-1} ampicillin, supplemented with or without SDS (0.5%) and EDTA (0.5 mM) as indicated, and incubated overnight at 37˚C. In the plasmids used, the *tol-pal* gene(s) is placed under the control of the T7 promoter, which is transcribed at low levels by endogenous polymerases. $tolR_{D23R}$ is a non-functional allele encoding TolR protein that is defective in transducing energy derived from the pmf (14).

Fig. S2. *tol-pal* mutations do not affect β-barrel OMP and LPS assembly. Immunoblot analyses of (*A*) indicated OMPs and (*B*) LPS in the OMs of WT and *tol-pal* strains. The OMP assembly mutants (*bamB*, *bamD*, Δ*surA*) and the LpxC-deficient (*lpxC*1272) or YciM-overexpressing (p*yciM*) strains (60) serve as controls for decreased OMP and LPS levels, respectively. The levels of LptE serve as a loading control.

Fig. S3. Inner and outer membranes of both WT and *tol-pal* strains are effectively separated via fractionation on sucrose density gradients. (*A*) [^{3}H]-distribution profiles of WT (*black circles*) and Δ*tolQ* mutant (*red triangles*) cell lysates fractionated on a sucrose density gradient. Cells were grown in the presence of [2-^{3}H]-glycerol to specifically label PLs in the IM and OMs. (*B)*

293 Percent NADH oxidase activity (*upper panel*) and LPS levels (*lower panel*) (dot blot) in pooled
294 IM and OM fractions from (*A*).
295
296 **Fig. S4.** Cells lacking the Tol-Pal complex contain more PLs in the OM, compared to the IM.
297 Representative [^{3}H]-distribution profiles of cell lysates from WT (*black circles*), *tol-pal* mutants
298 (*red triangles*), *tol-pal*-complemented strains (*blue inverted triangles*), and various control
299 strains, fractionated on sucrose density gradients. Cells were grown in the presence of [2-^{3}H]-
300 glycerol to specifically label PLs in the IMs and OMs. Total [^{3}H]-activities detected in IM (6-10)
301 and OM (12-14) fractions were expressed as a percentage of their sums, averaged across three
302 replicate experiments, and plotted in Fig. 2*A*.
303
304 **Fig. S5.** Cells lacking the Tol-Pal complex accumulate excess PLs (relative to LPS) in the OM.
305 (*A)* Workflow for differential extraction and subsequent quantification of PLs and LPS levels in
306 the [^{14}C]-acetate labelled OMs. (*B)* In-gel quantification of [^{14}C]-LPS levels in the OMs of WT,
307 *tol-pal* mutants, *tol-pal*-complemented strains, and various control strains. [^{14}C]-LPS of
308 respective strains separated on SDS-PAGE gels (*right*) were visualized by phosphor imaging and
309 quantified via densitometry using a linear standard curve (*left*). (*C*) Tabulation of [^{14}C]-labelled
310 PL levels (scintillation counts), LPS levels (gel densitometry), and arbitrary PL/LPS ratios in the
311 OMs of the indicated strains. The average PL/LPS ratio for each strain was obtained from three
312 independent experiments, and plotted in Fig. 2*B*.
313
314 **Fig. S6.** *tol-pal* mutants survive toxicity induced by overproduction of LpxC, the enzyme
315 catalyzing the first committed step in LPS biosynthesis. (*A)* Growth profiles of WT, Δ*tolQ* and

316 Δ*tolA* cells harboring either pBAD18cm empty vector (p) or pBAD18cm*lpxC* (p*lpxC*) and grown
317 in the presence of arabinose (0.2%). OD_{600} values were measured every hour during growth.
318 Error bars represent the standard deviation observed from triplicate experiments. (*B)* Indicated
319 serial dilutions of 0-, 4- and 7-h cultures of the same strains in (*A*) were spotted on LB agar
320 plates containing 30 μg ml^{-1} cam and incubated overnight at 37˚C.
321
322 **Fig. S7.** PG/CL is converted to PS in the absence of PSD function. TLC time-course analyses of
323 [^{32}P]-pulse-labelled PLs extracted from the IMs and OMs of the WT strain also harboring the
324 temperature-sensitive *psd2* mutation. Cells were incubated at the restrictive temperature (42˚C, 4
325 h) and PLs were pulse-labelled with [^{32}P]-phosphate during the last 30 min at the restrictive
326 temperature, and then chased in the presence of excess cold phosphate and hydroxylamine (HA;
327 10 mM) at the same temperature. HA is a known PSD inhibitor (34). The percentage levels of PE
328 (circles), PG/CL (squares), and PS (triangles) in the IM (grey symbols) and OM (white symbols)
329 at each time point were quantified and shown on the right. The results clearly showed
330 quantitative PG/CL to PS conversion.
331
332 **Fig. S8.** Cells lacking the Tol-Pal complex are defective in OM PG/CL turnover. Single time-
333 point TLC analyses of [^{32}P]-pulse-labelled PLs extracted from the IMs and OMs of indicated
334 strains also harboring the temperature-sensitive *psd2* mutation. Cells were incubated at the
335 restrictive temperature (42˚C, 4 h) and PLs were pulse-labelled with [^{32}P]-phosphate during the
336 last 30 min at the restrictive temperature, and then chased in the presence of excess cold
337 phosphate at the permissive temperature (30˚C) for 2 h. The average extents of PG/CL turnover

338 ([(%PG/CL)$_{start}$ – (%PG/CL)$_{2h}$]/[(%PG/CL)$_{start}$]) in the IM and OM for each strain was obtained
339 from three biological replicate (Reps) experiments, and plotted in Fig. 4.
340
341 **Fig. S9.** Although cells lacking the Tol-Pal complex accumulate ~50% more PLs in the OM, PL
342 compositions of this membrane are comparable to that in WT cells. TLC analysis of [^{14}C]-
343 labelled PLs extracted from the OMs of WT and indicated mutant strains. Equal amounts of
344 radioactivity were spotted for each sample. An unidentified lipid species that migrated in this
345 solvent system similarly to palmitoylated PG (65) is annotated by an asterisk (*). The percentage
346 levels of PE, PG/CL, and the unidentified lipid were quantified and shown below.
347
348 **Fig. S10.** Overexpression of OmpC-Mla components does not rescue SDS/EDTA sensitivity of
349 Δ*tolA* mutant. Serial dilutions of cultures of wild-type (WT) and the Δ*tolA* mutant strain (both in
350 the *psd2* background) harboring pBAD33 empty vector (pBAD) or pBAD33 encoding indicated
351 components of the OmpC-Mla system, were spotted on LB agar plates containing
352 chloramphenicol (30 μg ml^{-1}) and arabinose (0.2 %), supplemented with or without SDS (0.5%)
353 and EDTA (0.3/0.5 mM) as labeled, and incubated overnight at the permissive temperature
354 (30˚C).
355

Table S1. Bacterial strains used in this study.

Strains	Relevant genotype	References
MC4100	[*F⁻ araD139 Δ(argF-lac) U169 rpsL150 relA1 flbB5301 ptsF25 deoC1 ptsF25 thi*]	*51*
BW25113	*F- Δ(araD-araB)567 ΔlacZ4787::rrnB-3 λ- rph-1 Δ(rhaDrhaB)568 hsdR514*	*53*
NovaBlue	*endA1 hsdR17 (rK12– mK12+) supE44 thi-1 recA1 gyrA96 relA1 lac F' [proA+B+lacIqZΔM15::Tn10]*	Novagen
NR754	MC4100 *araD*$^{+}$	*24*
MR706	MG1655 *lpxC1272 leuB::Tn10*	*60*
EH150	*psd-2 purA*$^{+}$; temperature-sensitive PSD	*33*
NR1215	NR754 Δ*surA*	*61*
NR698	MC4100 *lptD4213* (*carB*$^{+}$, *Tn10*)	*62*
NR814	MC4100 *bamD::kan*	*63*
NR721	MC4100 *bamB::kan*	*62*
RS101	BW25113 Δ*tolQ::kan*	This study
JW0728	BW25113 Δ*tolR::kan*	*53*
RS102	BW25113 Δ*tolA::kan*	This study
JW5100	BW25113 Δ*tolB::kan*	*53*
RS104	BW25113 Δ*tol-pal::kan*	This study
RS105	BW25113 Δ*lpp::kan*	This study
RS119	MC4100 Δ*tolQ::kan*	This study
RS120	MC4100 Δ*tolR::kan*	This study
RS121	MC4100 Δ*tolA::kan*	This study
RS122	MC4100 Δ*tolB::kan*	This study
RS125	MC4100 Δ*tol-pal::kan*	This study
RS137	MC4100 Δ*lpp::kan*	This study
CZS011	MC4100 Δ*mlaC::kan*	Lab collection
RS173	EH150 Δ*tolR::kan*	This study
RS174	EH150 Δ*tolA::kan*	This study
RS177	EH150 *bamB::kan*	This study
RS178	EH150 Δ*mlaC::kan*	This study
RS180	EH150 Δ*tolA* Δ*mlaC::kan*	This study
JXE082	NR754 Δ*tolQ::kan*	This study
JXE081	NR754 Δ*tolA::kan*	This study

Table S2. Plasmids used in this study.

Plasmids	Description	Plasmid construction		References
		PCR template[a]	PCR primers[b]	
pET23/42	P_{T7} inducible expression vector, contains multiple cloning site of pET42a(+) in pET23a(+) backbone; Amp^R	-	-	*23*
pBAD18cm	P_{BAD} inducible expression vector; Cam^R	-	-	*64*
pBAD33	P_{BAD} inducible expression vector; Cam^R	-	-	*64*
pET23/42*tolQ*	Encodes full length TolQ; Amp^R	Ch. DNA	TolQ-N-NdeI/TolQ-C-AvrII	This study
pET23/42*tolR*	Encodes full length TolR; Amp^R	Ch. DNA	TolR-N-NdeI/TolR-C-AvrII	This study
pET23/42$tolR_{D23R}$	Encodes full length $TolR_{D23R}$; Amp^R	pET23/42*tolR*	TolR-D23R-N/TolR-D23R-C	This study
pET23/42*tolA*	Encodes full length TolA; Amp^R	Ch. DNA	TolA-N-NdeI/TolA-C-AvrII	This study
pET23/42*tolB*	Encodes full length TolB; Amp^R	Ch. DNA	TolB-N-NdeI/TolB-C-AvrII	This study
pET23/42*tol-pal*	Encodes full Tol-Pal complex; Amp^R	Ch. DNA	TolQ-N-NdeI/Pal-C-AvrII	This study
pBAD18cm*lpxC*	Encodes full length LpxC; Cam^R	Ch. DNA	LpxC-N-KpnI/LpxC-C-XbaI	This study
pDSW210-*yciM*	Encodes full length yciM under control of P_{trc}; IPTG-inducible; Amp^R	-	-	*60*
pBAD33*mlaA*	Encodes full length MlaA; Cam^R	Ch. DNA	MlaA-N-KpnI/MlaA-C-XbaI	This study
pBAD33*mlaFEDCB*	Encodes full length MlaFEDCB; Cam^R	Ch. DNA	MlaFEDCB-N-KpnI/MlaFEDCB-C-XbaI	This study

[a] Ch. DNA = MC4100 chromosomal DNA.

[b] Primer sequences are listed in Table S3.

360 **Table S3. List of oligonucleotides**

Primer name	Sequence (5'-3')[a]
TolQ-N-NdeI	AGCACATATGACTGACATGAATATCC
TolQ-C-AvrII	ATTCCTAGGTTACCCCTTGTTGCTCTC
TolR-N-NdeI	ACATCATATGGCCAGAGCGCGTGGAC
TolR-C-AvrII	ACACCTAGGTTAGATAGGCTGCGTC
TolA-N-NdeI	ACATCATATGTCAAAGGCAACCGAACAAAAC
TolA-C-AvrII	ACTACCTAGGTTACGGTTTGAAGTCC
TolB-N-NdeI	GCGAATTCATATGAAGCAGGCATTACGAGTA
TolB-C-AvrII	ACTACCTAGGTCACAGATACGGCG
Pal-C-AvrII	ACTACCTAGGTTAGTAAACCAGTACC
LpxC-N-KpnI	ATAAGGTACCTAATTTGGCGAGATAATACGATGATCAAA
LpxC-C-XbaI	ATCGTCTAGATTATGCCAGTACAGCTGAAGG
MlaA-N-KpnI	ATAAGGTACCAAAAAAACAGGGAGACATTTATGAAGCTTC
MlaA-C-XbaI	ATCGTCTAGATTATTCAGAATCAATATCTTTTAAAT
MlaFEDCB-N-KpnI	ATAAGGTACCCGCAAGACGAAGGGTGAATTATGGAGCAGT
MlaFEDCB-C-XbaI	ATCGTCTAGATTAACGAGGCAGAACATCAGCAGG
TolR-D23R-N	ATTGTACCGTTGCTGAGAGTACTGCTGGTGCTG
TolR-D23R-C	CAGCACCAGCAGTACTCTCAGCAACGGTACAAT

361 [a] restriction sites are underlined.

Supplementary Figures

Figure S1

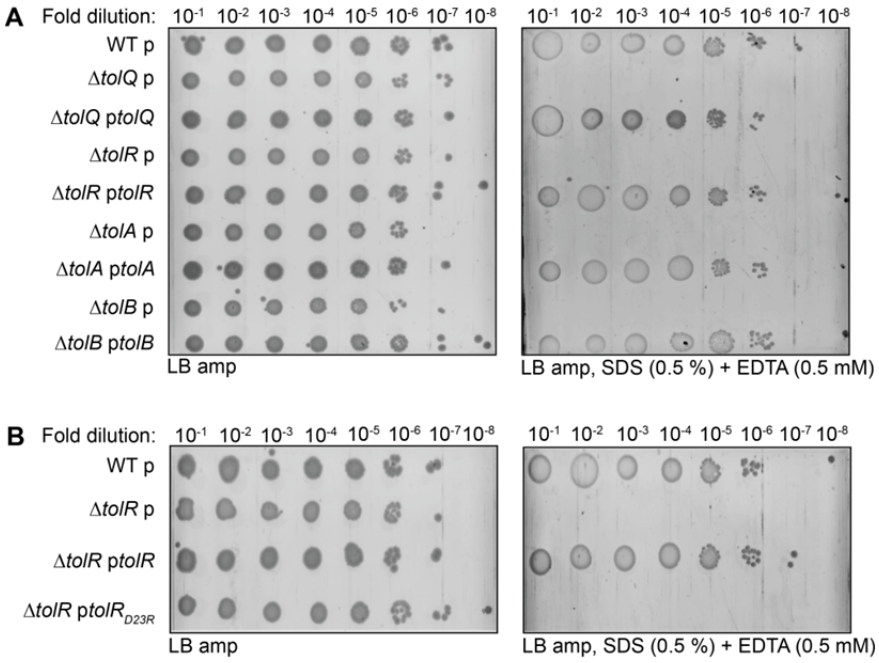

365 **Figure S2**

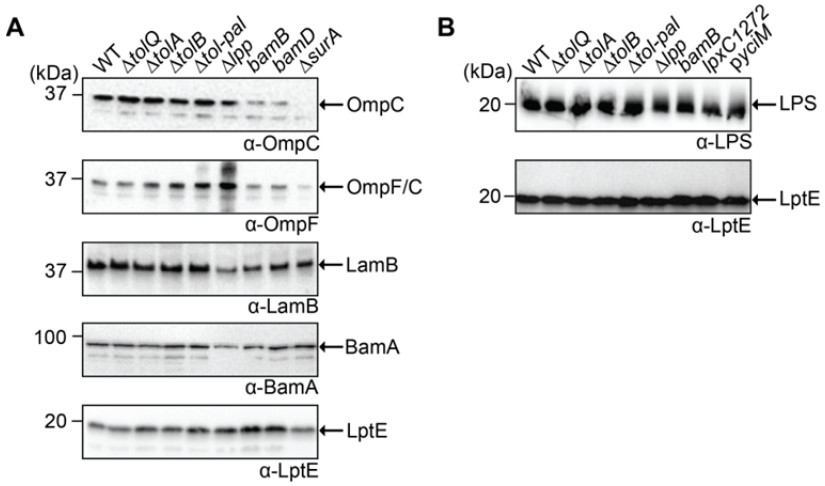

366

Figure S3

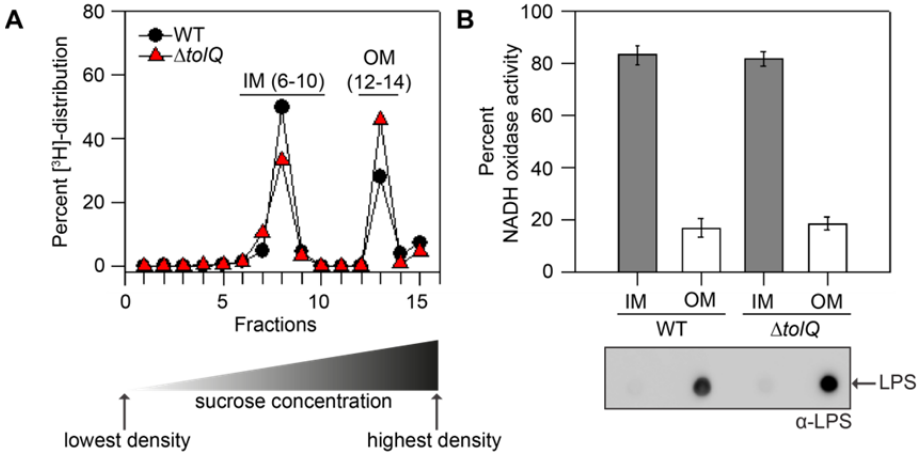

Figure S4

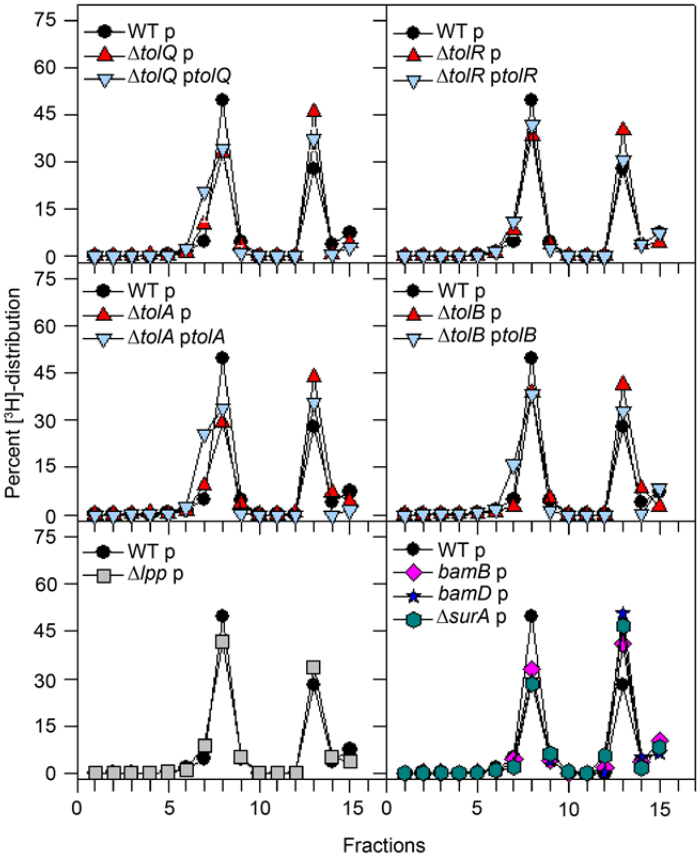

Figure S5

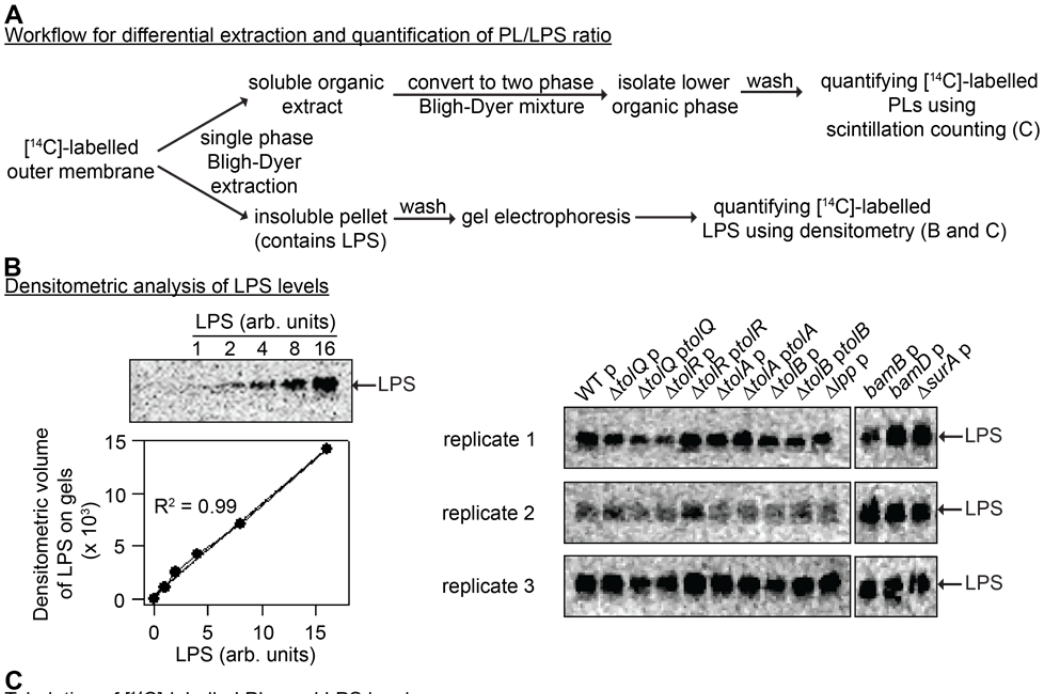

C
Tabulation of [14C]-labelled PLs and LPS levels

Strains	Replicate 1			Replicate 2			Replicate 3			Average	
	PL	LPS	PL/LPS	PL	LPS	PL/LPS	PL	LPS	PL/LPS	PL/LPS	SD
WT p	3640	7.3	497	1517	2.5	597	3602	7.9	457	517	72
Δ*tolQ* p	3715	4.3	860	3014	3.1	975	6471	8.1	797	877	91
Δ*tolQ ptolQ*	1970	3.0	663	1321	2.4	548	1990	4.4	457	556	103
Δ*tolR* p	3448	2.6	1306	3452	2.7	1279	6215	5.6	1110	1231	106
Δ*tolR ptolR*	6076	9.2	661	2147	4.1	526	6062	10.5	577	588	68
Δ*tolA* p	5342	5.6	961	2971	2.7	1092	5218	7.4	709	921	195
Δ*tolA ptolA*	3508	8.6	406	1987	2.9	688	4250	6.2	691	595	163
Δ*tolB* p	3672	4.4	838	2214	2.6	868	3300	4.2	782	830	44
Δ*tolB ptolB*	4184	4.2	1006	3014	3.2	957	3890	6.4	610	857	216
Δ*lpp* p	2871	5.0	578	1784	3.0	599	3362	6.4	524	567	38
bamB p	6622	2.8	2340	6806	6.2	1105	6624	7.0	944	1463	764
bamD p	5784	7.7	753	6188	6.3	985	6252	5.5	1143	960	196
Δ*surA* p	7004	5.0	1401	7314	6.8	1076	7528	6.1	1236	1238	163

373 **Figure S6**

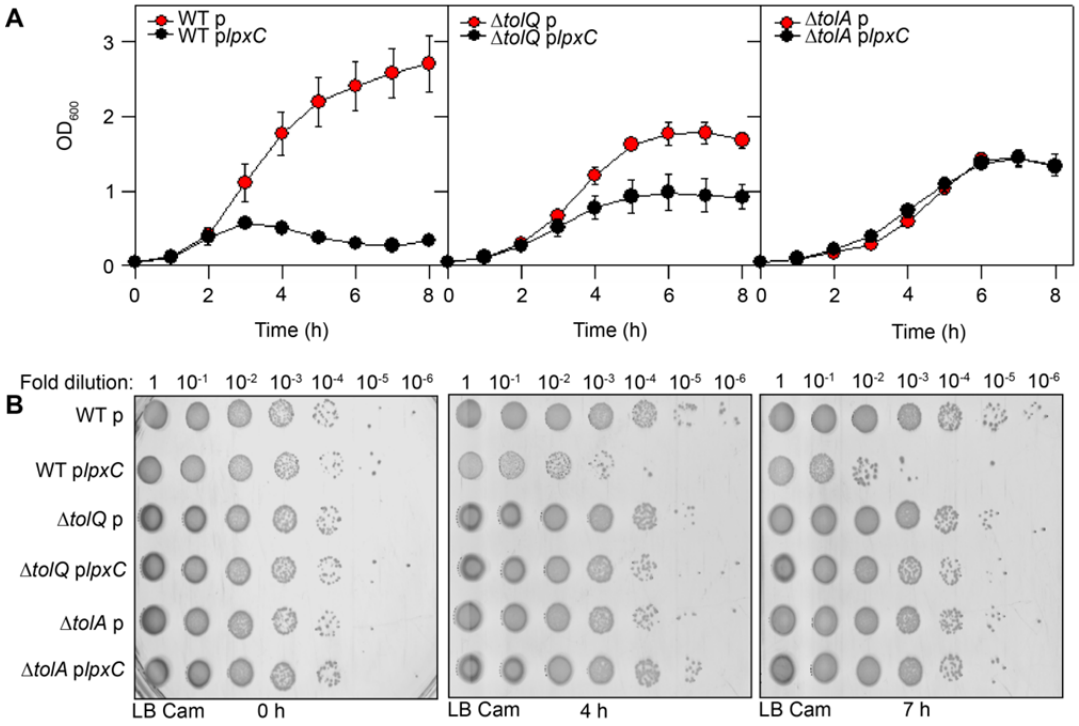

374

375 **Figure S7**

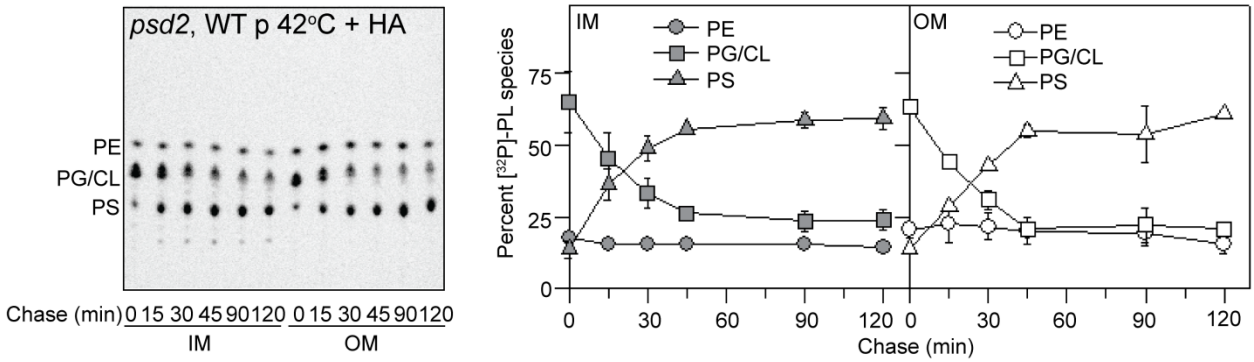

376

Figure S8

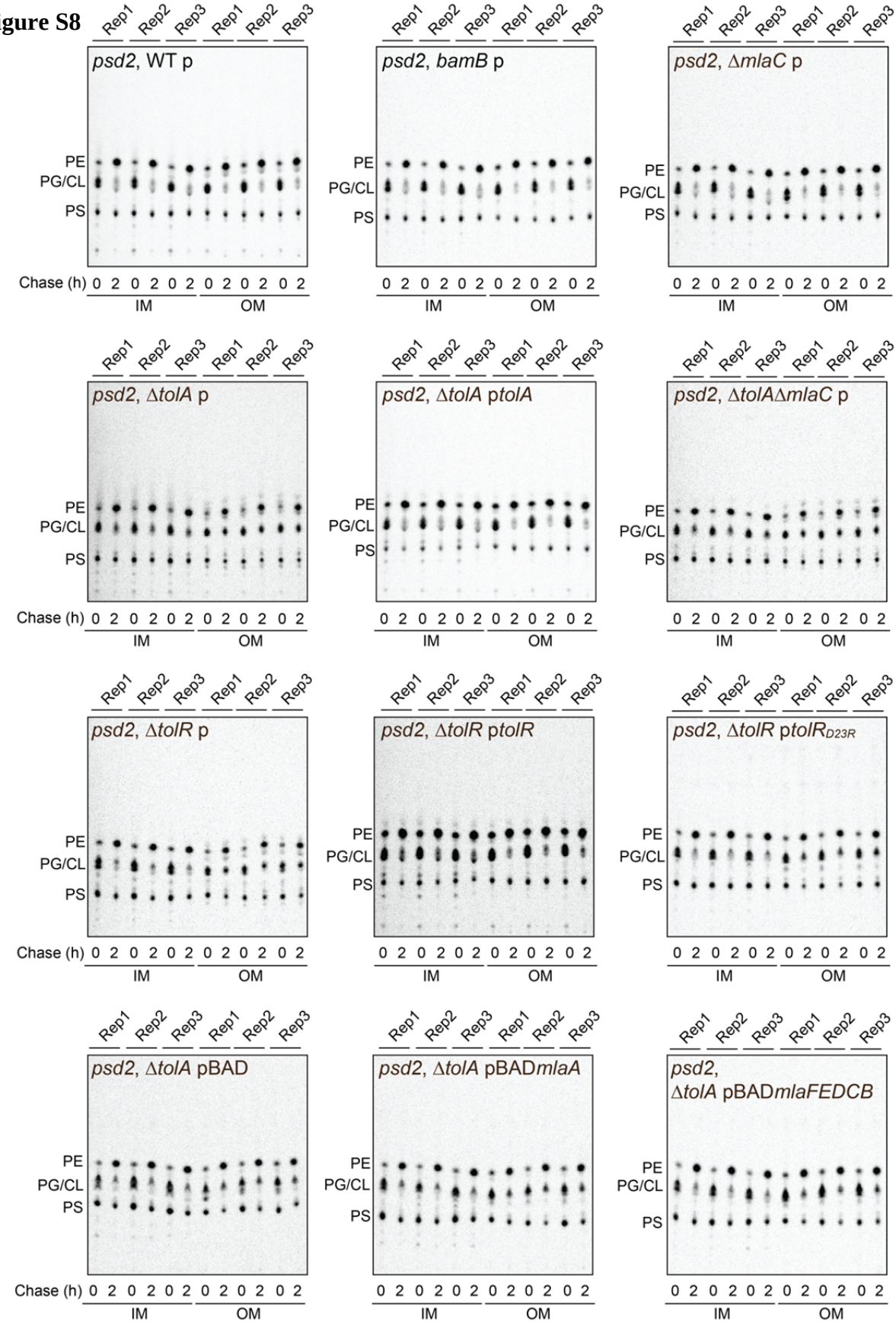

377

378 **Figure S9**

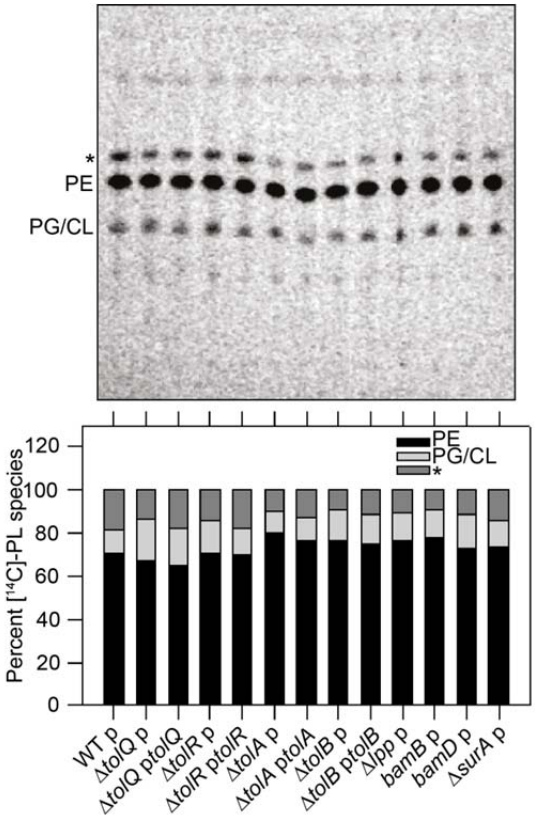

379

380 **Figure S10**

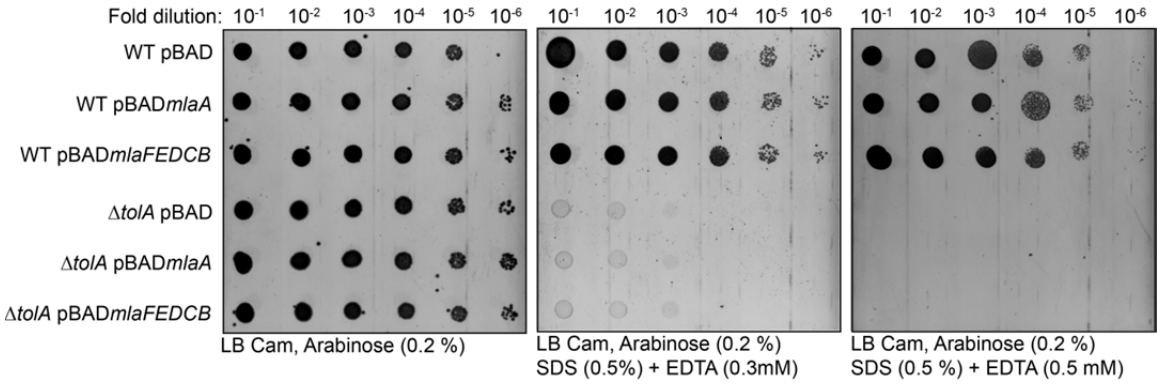

381